Available online at www.sciencedirect.com
SCIENCE DIRECT®
International Journal of Multiphase Flow 30 (2004) 735–761
International Journal of Multiphase Flow
www.elsevier.com/locate/ijmulflow

The effect of channel diameter on adiabatic two-phase flow characteristics in microchannels ☆

P.M.-Y. Chung, M. Kawaji *

Department of Chemical Engineering and Applied Chemistry, University of Toronto, Toronto, Ont., Canada M5S 3E5

Received 9 March 2003; received in revised form 22 April 2004

Abstract

The effect of channel diameter on two-phase flow was investigated to identify the phenomena which distinguish microchannels from minichannels. Experiments were conducted with a mixture of nitrogen gas and water in circular channels of 530, 250, 100, and 50 μm diameter. The temperature, pressure and flow rates of the liquid and gas were measured and images of the flow patterns recorded. The two-phase flow was characterized by the flow regime map, void fraction, and frictional pressure drop. In the 530 and 250 μm channels, the two-phase flow characteristics were similar to those typically observed in minichannels of ~1 mm diameter. In the 100 and 50 μm channels, the two-phase flow behaviour departed from that observed in minichannels—the occurrence of slug flow dominated, the void fraction–volumetric quality relationship departed from a linear Armand-type correlation, and mass flux no longer influenced the two-phase frictional multiplier. Clearly, the channel diameter has an effect on two-phase flow in the range of channel diameters investigated. A new slug flow model is also proposed to gain physical insight into the observed flow characteristics in microchannels. The model can predict the two-phase frictional pressure gradient for the 100 and 50 μm channels, if the actual void fraction data are used, substantiating the assumed flow mechanism.

Keywords: Microchannel; Gas–liquid flow; Microfluidics; Flow patterns; Void fraction; Pressure drop; Liquid film; Ring film; Capillary tube

☆ The authors would like to dedicate this paper to Professor George Yadigaroglu on the occasion of his 65th birthday. One of the authors (MK) was introduced to the field of two-phase flow in two graduate courses taught by George in 1979 at UC Berkeley. George also took on MK as a graduate student to work on a research project on rewetting phenomena shortly before moving to Greece and later to Switzerland. As a result, George has directly and indirectly helped shape the research careers of both of us in the field of two-phase flow. A happy 65th birthday.

* Corresponding author. Tel.: +1-416-978-3064; fax: +1-416-978-8605.
E-mail address: kawaji@ecf.utoronto.ca (M. Kawaji).

0301-9322/$ - see front matter
doi:10.1016/j.ijmultiphaseflow.2004.05.002

1. Introduction

The technology to fabricate microchannels has quickly evolved from the miniaturization of traditional machining techniques (milling and sawing) to the adoption of modern techniques (anisotropic wet chemical etching, dry plasma etching and surface micromachining) used in the semiconductor manufacturing industry (Kandlikar and Grande, 2003). The fabrication technology is available to make microchannels with volumes of fluid in the order of nanoliters or picoliters (Madou, 2002). Intensive research is underway to understand the movement of liquids and gases in these microscaled structures—microfluidics.

While the single-phase flow of liquid or gas in microchannels has been a topic of interest for over a decade, the two-phase flow of liquid and gas is less understood, since the hydraulic diameter (D_H) of a so-called microchannel for two-phase flow has been mostly limited to a diameter of about 1 mm in the literature. Few two-phase flow studies are available that involve a channel diameter of 100 μm or less.

Kawahara et al. (2002) recently investigated the two-phase flow of nitrogen gas and water through a 100 μm circular channel oriented horizontally. They reported significant differences in the flow regime maps and void fraction data from those previously described for minichannels with $D_H \sim 1$ mm. In particular, they reported the existence of flow patterns unique to microchannels (liquid-ring flow and serpentine-like gas core flow) and deviation of void fraction data from a linear Armand-type correlation normally applicable to minichannels with $D_H \sim 1$ mm. Chung et al. (in press) further compared the flow characteristics in a 96 μm square channel to that in a 100 μm circular channel for a mixture of nitrogen gas and water. They reported that the channel shape did not affect the two-phase pressure drop and void fraction, but the ring-shaped liquid film became smooth as the cross section changed from circular to square.

Air–water two-phase flow experiments have also been conducted in 25 and 100 μm circular microchannels (Feng and Serizawa, 1999; Serizawa and Feng, 2001; Serizawa et al., 2002). Five flow patterns were observed: dispersed bubbly flow, gas slug flow, liquid-ring flow, liquid lump flow, and liquid droplet flow. The occurrence of liquid-ring flow and liquid lump flow indicated differences in the flow patterns between microchannels of $D \leqslant 100$ μm and minichannels of $D \geqslant 1$ mm, but at what diameter the flow characteristics change has yet to be determined. Serizawa et al. (2002) reported that the void fraction data agreed with the Armand (1946) correlation.

Earlier, Stanley et al. (1997) investigated two-phase pressure drop and heat transfer in square and rectangular aluminum channels of hydraulic diameters ranging from 56 to 256 μm. They mixed water with argon, helium or nitrogen gas to vary the viscosity, density and surface tension of their fluid system, and reported that the conventional semi-empirical correlations for two-phase pressure drop over-predicted their microchannel data substantially.

As mentioned above, the available data for two-phase flow in microchannels with $D_H < 100$ μm are not entirely consistent and the effect of reducing the channel diameter on two-phase flow remains unclear (see a review by Kawaji and Chung, in press). Some results for microchannels differed from those in conventional channels, while others remained the same. Bubbly and droplet flows patterns have not always been observed in microchannels, even among the results for the same channel diameter. The departure and adherence of the void fraction data in microchannels to the Armand (1946) correlation applicable to minichannels of $D_H \sim 1$ mm have been both re-

ported. The two-phase frictional pressure drop in microchannels was best fitted by different researchers to both the homogeneous and separated flow models.

Hence, the objective of this work was to identify the changes that arise in two-phase flow characteristics due to a reduction in the channel diameter from 530 to 50 μm. In this experimental investigation, the two-phase flow structures were studied by flow visualization, a two-phase flow regime map was developed and the void fraction and frictional pressure drop data were correlated. The same experimental apparatus and approach were used on each size of channel so that any differences between two-phase flows in microchannels and minichannels can be attributed solely to the effect of channel diameter. In this paper, the latest research on the hydrodynamics of gas–liquid two-phase flow in channels with $D_H \ll 1$ mm is reviewed first, followed by a description of the present experimental work and results. The characteristics of the two-phase flow in a microchannel are then interpreted from the measured void fraction data and supported by a new theoretical model that uses the void fraction data to predict the two-phase frictional pressure gradient.

1.1. Two-phase flow characteristics in microchannels

1.1.1. Two-phase flow patterns and flow pattern maps

There is still little systematic information available on the two-phase flow patterns in a microchannel. Feng and Serizawa (1999), Serizawa and Feng (2001), and Serizawa et al. (2002) reported observing five flow patterns in 25 and 100 μm diameter channels: dispersed bubbly flow, gas slug flow, liquid-ring flow, liquid lump flow, and liquid droplet flow. In a 100 μm circular channel and 96 μm square channel, Kawahara et al. (2002) and Chung et al. (in press) identified slug flow, liquid-ring flow, gas core flow surrounded by a serpentine-like liquid film, and semi-annular flow, but did not observe the dispersed bubbly and liquid droplet flows.

The observation of a liquid-ring flow pattern, however, appears to be unique to flow channels with $D_H \leqslant 100$ μm. With an increase in the gas flow rate, the liquid bridge between two consecutive gas slugs becomes unstable and a transition appears to take place from slug flow to liquid-ring flow. This liquid-ring flow pattern has not been observed before in capillary tubes of ~1 mm diameter by various authors (Fukano and Kariyasaki, 1993; Damianides and Westwater, 1988; Triplett et al., 1999; Zhao and Bi, 2001a).

Stanley et al. (1997) examined two-phase flow in square and rectangular microchannels with $D_H = 56 \sim 256$ μm. They tested various combinations of water with argon, helium or nitrogen gas. Without conducting any flow visualization, they plotted their measured flow rates on the flow regime maps of Baker (1954) and Suo and Griffith (1964) to deduce the presence of bubbly–slug, slug and annular flow. They reasoned that mist flow could not occur, as a result of the low quality. This method of deducing the flow patterns, however, assumes the applicability of macro-scale flow pattern maps to microscale data.

Only few experimental studies have presented the two-phase flow pattern maps for microchannels. Serizawa et al. (2002) constructed a flow pattern map for air–water flow in a 20 μm circular microchannel. They distinguished regions of bubbly flow, slug flow, liquid-ring flow, and liquid lump flow. Liquid droplet flow was omitted from this flow pattern map. Kawahara et al. (2002) developed a flow pattern map for nitrogen gas–water two-phase flow in a 100 μm circular microchannel. They identified regions of slug–ring flow, ring–slug flow, semi-annular flow, and

multiple flow. Chung et al. (in press) presented the flow pattern map for the same nitrogen gas–water flow in a 96 μm square microchannel. The same flow patterns observed by Kawahara et al. (2002) in the 100 μm circular channel were detected in the 96 μm square channel, accompanied by a shift in the transition boundaries for the ring–slug flow.

1.1.2. Void fraction

Measurements of the void fraction in microchannels are still scarce. Serizawa et al. (2002) applied an image analysis technique to the high-speed video recordings and obtained the average void fraction for an air–water mixture in a 20 μm capillary tube. The gas bubbles and slugs in the recorded pictures were assumed to have a symmetrical body, however, liquid-ring flow was not included in the void fraction measurements despite having a symmetrical shape. When plotted against the volumetric quality (or homogeneous void fraction), β, the void fraction behaved like that estimated by the linear Armand correlation (1946). In contrast, Kawahara et al. (2002) and Chung et al. (in press) measured the void fractions in a 100 μm circular channel and 96 μm square channel, respectively, both of which demonstrated a strong deviation of the void fraction–volumetric quality relationship from that predicted by Armand (1946).

1.1.3. Frictional pressure drop

There are even fewer studies that have experimental data for the two-phase frictional pressure drop in a microchannel. Stanley et al. (1997) found the predictions of the two-phase pressure drop using the homogeneous flow model to be reasonable, while those for the separated flow model to behave poorly for square and rectangular microchannels with hydraulic diameters ranging from 56 to 256 μm. On the other hand, Kawahara et al. (2002) showed the two-phase frictional pressure drop in a 100 μm circular channel to be better predicted by a separated and not homogeneous flow model. Chung et al. (in press) confirmed this success for a 96 μm square channel.

2. Experimental details

What follows is a brief description of the apparatus and flow conditions for experiment.

2.1. Experimental apparatus and test conditions

Details of the experiment are explained in brief. The reader can refer to Kawahara et al. (2002) and Chung et al. (in press) for pertinent information about the experiment not specified here. Fig. 1 illustrates the experimental apparatus used. Liquid was driven through the horizontal microchannel by a pneumatic-type pump that consisted of a pressure vessel filled with de-ionized water and connected to a nitrogen gas cylinder. A gas supply is necessary to drive the liquid out of the pressure vessel and to mix with the liquid in the microchannel. In Fig. 1, the nitrogen gas from a single cylinder serves both purposes. Under some circumstances, a second gas cylinder was used to provide gas for the two-phase mixture. It was easier to hold the flow rate of the liquid constant, while increasing that of the gas by employing two gas cylinders.

A gas–liquid mixture was pumped into a given microchannel positioned horizontally. Nitrogen gas was selected for the gas phase because it is practically insoluble in water. To compare the

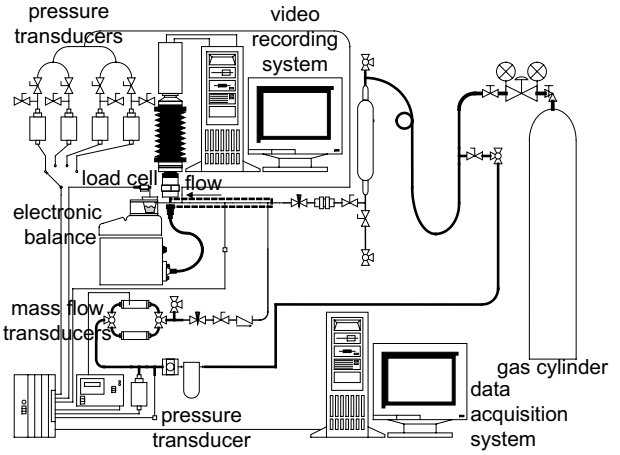

Fig. 1. Experimental apparatus.

pressure drop data for single-phase flow with those documented in the literature, de-ionized water was selected as the liquid. The purified water (Milli-Q Water System from Millipore) had a specific conductance of 0.1 μmho/cm. Fig. 2 provides a closer look near the test section. Four circular channels (capillary tubing made of fused silica with standard polyimide coating from Polymicro Technologies) with inner diameters of 49.5, 100, 250 and 526 μm were used for the test section, as listed in Table 1. The inner walls of the capillary tubes were hydraulically smooth as viewed under a scanning electron microscope.

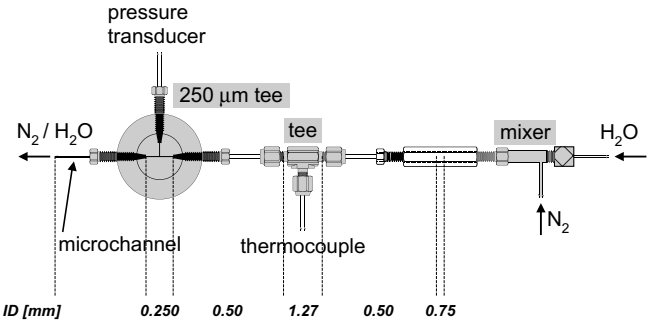

Fig. 2. Test section.

Table 1
Microchannel dimensions

Channel cross-section	D (μm)	L (mm)
Circular	49.5	46.0
Circular	99.6	63.9 and 65.1
Circular	250	156.7
Circular	526	277

Long channels of large L/D ratios ($527 \leqslant L/D \leqslant 929$) were purposely used to diminish the entrance and exit effects. Thus, the viewing window was always located near the rear of each channel by stripping the polyimide cladding around the fused silica core over a 10 mm length.

Three pressure transducers (PX303 and PX725 series from Omega) covering different ranges (3450 ± 8.6, 210 ± 0.52 and 24.9 ± 0.037 kPa,) were connected to a tee junction upstream of the microchannel inlet to measure the pressure drop between the channel inlet and outlet for two-phase flow. Three additional pressure transducers (PX303 and PX120 series from Omega and model ABH200PSC1B from Honeywell) of various ranges ($13{,}790 \pm 34$, 170 ± 2 and 1380 ± 3.4 kPa) were also used for single-phase liquid flow. The tee junction had an internal diameter of 250 μm and was connected to the incoming line carrying two-phase flow on the right, the test section on the left and the manifold of pressure transducers at the top. The liquid was discharged freely from the test section, so that the pressure was atmospheric and temperature ambient at the microchannel outlet. A type K thermocouple probe (model GKMQSS-062U-12 from Omega) was used to measure the two-phase temperature upstream of the microchannel.

The liquid flow rate was determined by using an electronic balance (120 ± 0.001 g, model VI-1mg from Acculab) or load cell (50.97 ± 0.255 g, model ELJ-0.5N from Entran Devices) to weigh the discharge liquid collected over time. The gas flow rate was measured using three mass flow meters (model 179A-23012 from MKS Instruments, and models 8172-0411 and 8172-0451 from Matheson Gas Products) to encompass a wide range of conditions (1 ± 0.01, 10 ± 0.1 and 50 ± 0.5 sccm). The analog signals for all of the pressure, temperature and mass flow rate readings were sampled at 100 Hz by a 16-bit data acquisition system (model NI 6035E from National Instruments).

As depicted in Fig. 3, the two-phase mixer (model FSMUAS1.5 from Valco International Co. Inc.) consisted of an internal core passage for liquid and an external annular passage for gas. Liquid flowed axially through a 500 μm tube, while gas flowed peripherally through a 200 μm

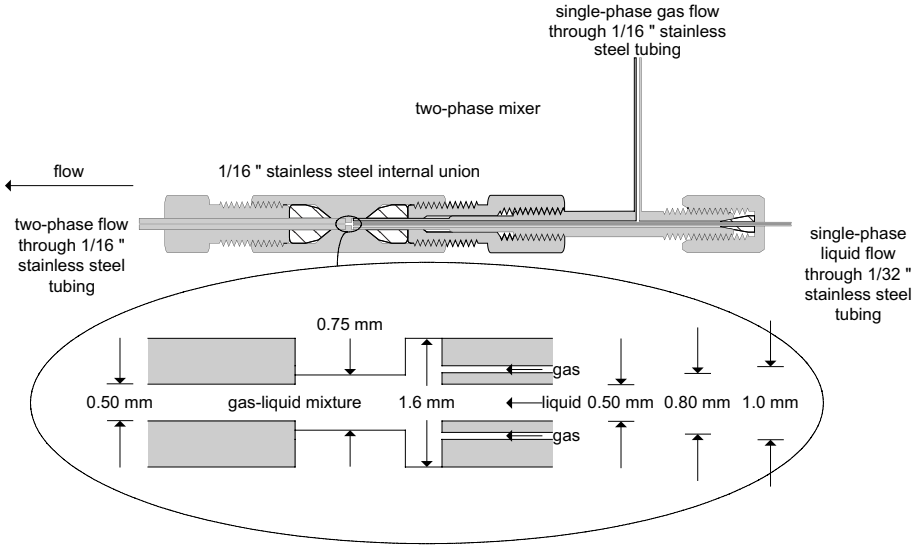

Fig. 3. Two-phase flow mixer.

annular gap. Eventually, the two streams mixed by flowing collectively into a 500 μm ID/1/16 in. OD tube that was connected to the tee fitting for pressure measurements upstream of the test section. Beyond the tee fitting, the newly formed two-phase flow entered the microchannel.

Background illumination to see the flow patterns was generated by a cold lamp (model DCR III from Schott-Fostec) located behind the test section. The view field was magnified by attaching a 5X microscope objective lens (model 378-802-2 from Mitutoyo America Corporation) to the video camera. Two monochrome CCD cameras were used interchangeably. The first video camera (model TM-1040 from Pulnix America) had a resolution of 1024 (H) × 1024 (V) pixels and recorded at a maximum frame rate of 30 fps and shutter speed of 1/16,000 s. The second video camera (model ES310 Turbo from Roper Scientific MASD) had a resolution of 648 (H) × 484 (V) pixels and recorded at a maximum frame rate of 125 fps and minimum exposure period of 66 μs.

The problem of optical distortion was dealt earlier by Kawahara et al. (2002). They elected to not correct for optical distortion so that the images of the gas–liquid interfacial structure near the channel wall could be enlarged and better examined. Likewise, optical distortion is not addressed here for the same reason.

Throughout the experiment, the mixture temperature at the channel inlet was maintained between 22.9 and 29.9 °C. The mixture was free to discharge at the channel outlet so that the two-phase pressure at exit was atmospheric. The experiment covered a range of $0.01 \leqslant j_L \leqslant 5.77$ m/s for the superficial liquid velocity and $0.02 \leqslant j_{G,AVG} \leqslant 72.98$ m/s for the average superficial gas velocity. The ranges of dimensionless parameters relevant to the present two-phase microchannel flow experiment are the Bond number ($0.000083 \leqslant Bo \leqslant 0.0095$), the superficial Weber number for liquid ($0.00057 \leqslant We_{LS} \leqslant 116$) and gas ($0.0000020 \leqslant We_{GS} \leqslant 12$), the superficial Reynolds number for liquid ($2 \leqslant Re_{LS} \leqslant 2300$) and gas ($0.4 \leqslant Re_{GS} \leqslant 751$) and the capillary number ($0.00013 \leqslant Ca_L \leqslant 0.070$). These values indicate the relative significance of the forces in the flow field (inertia > surface tension > viscous force > gravity).

It is also noted that with decreasing channel size, the Bond number, the superficial Reynolds numbers, the Weber number, and the capillary number all decrease. Hence, the following generalization about the relative forces in channels of decreasing diameter can be made: the gravitational force and inertia are diminished, while the surface tension effect and viscous force are intensified. The trend in the capillary number for smaller channels also implies that the viscous force grows stronger than the effect of surface tension.

2.2. Data analysis

The method used to calculate the two-phase frictional pressure drop is described below. The reader is referred to Kawahara et al. (2002) for further details on determining the frictional pressure drop for single-phase liquid flow and two-phase gas–liquid flow. The assumptions made to simplify the pressure drop calculations are indicated there, too.

Initially, experiments were conducted with de-ionized water to calculate the single-phase friction factor from the frictional pressure drop. Afterward, the computed friction factor was compared with the conventional value for laminar flow in a pipe. The two-phase frictional pressure drop was calculated by subtracting estimates of the pressure drop due to inlet contraction and flow acceleration from the total pressure drop measured in the horizontal channel. To estimate the pressure drop attributed to acceleration of the flow, the experimental void fraction was evaluated

Table 2
Measurement uncertainties

Parameters	Uncertainty range
Mass flow rate of liquid, m_L	±0.1 to ±1%
Mass flow rate of gas, m_G	±1 to ±10%
Superficial liquid velocity, j_L	±2.1 to ±3%
Superficial gas velocity, j_G	±3 to ±12%
Void fraction, ε	−0.05 to −0.01
Total two-phase pressure gradient, $(\Delta P/\Delta Z)$	±1 to ±4%
Two-phase frictional pressure gradient, $(\Delta P_f/\Delta Z)_{TP}$	±2 to ±7%
Two-phase friction multiplier, ϕ_L^2	±2 to ±7%

from the analysis of the video recordings and fitted to either the Armand correlation (1946) or a recent empirical correlation for microchannels suggested by Kawahara et al. (2002).

The measurement uncertainties for the present experiments were estimated using a propagation of error analysis (Kline and McClintock, 1953), and the results are summarized in Table 2.

3. Results and discussion

The experimental results are presented now on the two-phase flow patterns, void fraction and two-phase frictional pressure drop. Whenever possible, these results will be compared against those available in the published literature and any disagreement with the measured results clarified.

3.1. Two-phase flow patterns

The images of the two-phase flow were analyzed and flow patterns categorized in accordance with the flow patterns defined by Triplett et al. (1999) for a minichannel and Kawahara et al. (2002) for a microchannel.

3.1.1. Minichannel flow patterns

All of the flow patterns observed in the 250 and 530 μm diameter channels were found to correspond to those associated with minichannels ($D_H \approx 1$ mm), as described by Triplett et al. (1999) for air–water two-phase flow in horizontal circular minichannels of 1.09 and 1.45 mm diameter. See Fig. 4 for images of the flow patterns recorded in the 250 μm circular channel. However, only variants of the slug flow regime could be seen in the 50 and 100 μm diameter channels. Bubbly, churn, slug–annular and annular flow could no longer be identified in those microchannels.

Bubbly flow is recognized by the passage of spherical bubbles smaller than the channel diameter (Fig. 4a). With smaller channels, the size of bubble for bubbly flow decreases, and as a result of the surface tension effect, the non-spherical bubbles of Triplett et al. (1999) are absent.

Elongated cylindrical bubbles longer than the channel diameter are a feature of plug and slug flow patterns (Fig. 4b). The gas slug can be extremely long under a flow condition of low liquid and high gas superficial velocities. In a single recorded image, it may resemble annular flow with a

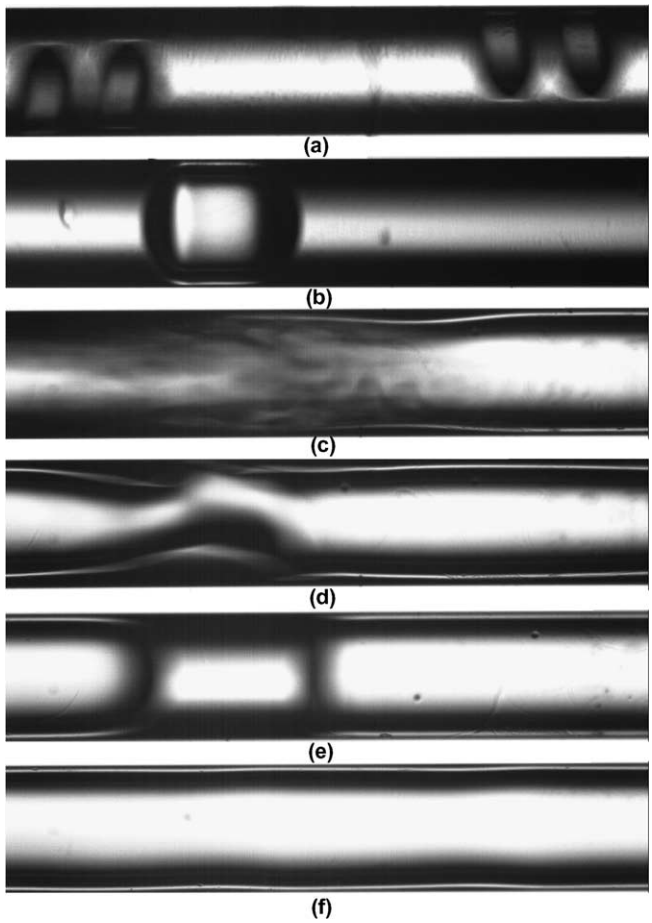

Fig. 4. Two-phase flow patterns in a 250 μm microchannel under different flow conditions: (a) bubbly flow at $j_L = 0.99$ m/s and $j_G = 0.27$ m/s; (b) slug flow at $j_L = 0.055$ m/s and $j_G = 13.61$ m/s; (c) swirling pattern in churn flow at $j_L = 4.25$ m/s and $j_G = 5.71$ m/s; (d) serpentine-like gas core in churn flow at $j_L = 4.25$ m/s and $j_G = 5.71$ m/s; (e) liquid bridge in slug–annular flow at $j_L = 0.16$ m/s and $j_G = 15.71$ m/s; (f) annular flow at $j_L = 0.015$ m/s and $j_G = 12.65$ m/s.

gas core and smooth liquid film, but an image of a liquid bridge or liquid slug would eventually appear in the sequence of images to signify the ending of the gas slug. A notable consequence of scaling down the channel diameter is that the gas slugs in a microchannel seem to occupy the entire cross section of the channel, unlike those in a large channel. Moreover, the gas slug in a minichannel has a less round nose and tail than that in a microchannel.

In the 250 μm channel, churn flow (Fig. 4c) displayed streaks and swirls that trail the gas slug, but not the highly irregular gas–liquid interfacial structure observed in minichannels which indicates the high level of mixing between the two-phases. Triplett et al. (1999) suggested the shedding of small bubbles at the tail of the gas slug and churning waves disturbing the wavy-annular flow as two factors that can lead to the creation of churn flow in minichannels. Note that the characteristics of churn flow in a minichannel should not be confused with those of churn flow

in a large pipe, as normally indicated by distorted bubbles of irregular shape and chaotic oscillations.

Additionally, the two-phase flow in the 250 and 530 μm channels showed interfacial structures resembling a serpentine-like gas core moving through the liquid (Fig. 4d). This flow pattern has not been observed in ~1 mm minichannels, but looks similar to the disturbed core-annular flow or corkscrew core flow occurring in conventional pipes for oil–water liquid–liquid flow (Joseph et al., 1997). The meandering motion of the gas core is a feature also observed in smaller microchannels. Furthermore, the deformed liquid film about the serpentine-like gas core may appear as the liquid lump flow first reported by Serizawa et al. (2002) for air–water flow in microchannels of 20, 25 and 100 μm diameter.

As shown in Fig. 4e, the liquid bridge separating the gas slugs occurs less frequently at higher gas flow rates. Instead, the gas slugs coalesce to produce a single gas slug with a distinctive neck. The interfacial waves that form the neck of the gas slug are large in amplitude and not regularly spaced. Triplett et al. (1999) named the flow pattern slug–annular flow as an intermediate between slug flow and annular flow.

Annular flow exists when the gas superficial velocity is sufficiently high. Consequently, annular flow can be recognized by the high void fraction and appears as a continuous gas core uninterrupted by a liquid bridge or liquid slug (Fig. 4e). The liquid film in annular flow has both a smooth and wavy surface. In Fig. 4f, the waves are shallow and long.

A characteristic of two-phase flow in microchannels is the occurrence of more than one flow pattern for a given flow condition and at the same location in the channel. Such a flow condition can be designated by a flow pattern that is either most probable or occurs in sufficient numbers. The run depicted in Fig. 5 is considered as churn flow, despite the appearance of other flow patterns at the same location but different times.

3.1.2. Flow pattern maps for horizontal minichannels

Fig. 6 presents the two-phase flow pattern maps developed for the 530 and 250 μm channels, in terms of the superficial velocities of liquid and gas. The flow regions in the figure were categorized by the definitions used for minichannels with $D_H \approx 1$ mm. In Fig. 6, the solid lines represent the boundaries at which transition occurred among the bubbly, slug, churn, slug–annular and annular flows. The same set of flow patterns were observed in both channels, but some of the transition boundaries (slug to churn and slug to slug–annular) were slightly shifted to lower j_G values as the channel diameter was reduced.

These flow pattern maps compared favorably with other maps developed previously for air–water two-phase flow in minichannels oriented horizontally and vertically. Triplett et al. (1999) showed five flow patterns in a horizontal circular channel having a 1.1-mm diameter: bubbly, slug, churn, slug–annular and annular flows. Fig. 7 compares the present flow pattern maps for the 530 and 250 μm channels with that obtained by Triplett et al. (1999) for a 1.1 mm minichannel. The broken lines represent the flow regime transition boundaries observed in the minichannel and the names of the flow patterns indicated on the figures are those given by Triplett et al. (1999).

There is much resemblance between the flow pattern maps for the 530 and 250 μm circular channels and that obtained by Triplett et al. (1999) for the 1.1 mm circular channel, which is representative of two-phase flow pattern maps for minichannels. The locations of the present flow patterns generally correspond well with those on their flow pattern map.

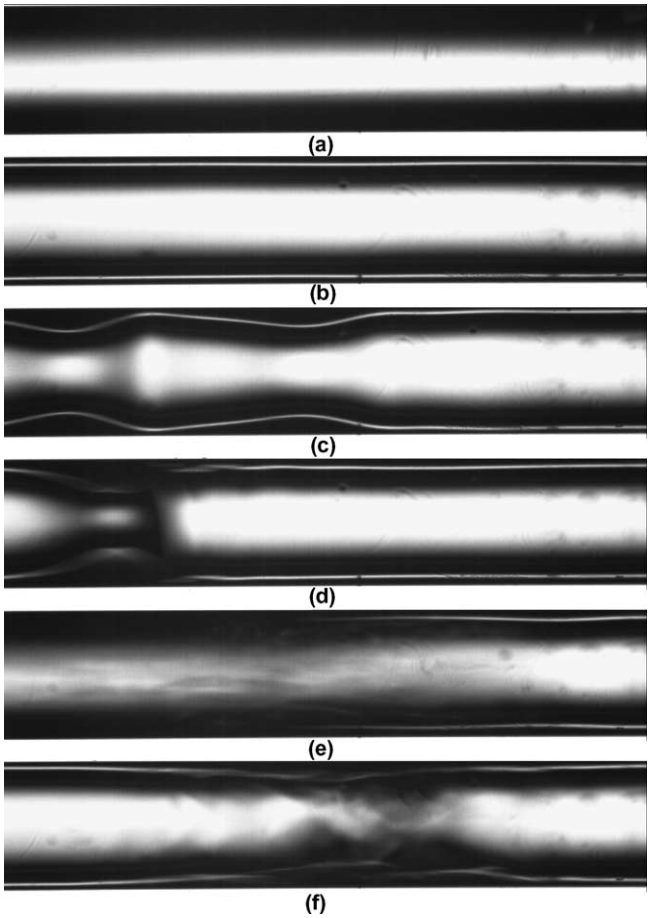

Fig. 5. Two-phase flow patterns in a 250 μm microchannel for the same flow condition ($j_L = 4.25$ m/s and $j_G = 5.71$ m/s): (a) single-phase liquid; (b) gas core with a thin-smooth liquid film; (c) gas core with a wavy liquid film; (d) gas core with a wavy liquid film; (e) streaked pattern; (f) serpentine-like gas core.

3.2. Microchannel flow pattern definitions

Bubbly, churn, slug–annular and annular flow appearing in both the 530 and 250 μm channels were absent and only some variations of slug flow were observed in the 100 and 50 μm channels. Typical flow patterns observed in the 50 μm channel are shown in Fig. 8. Mostly, gas slugs were observed surrounded by a thin or thick-smooth liquid film, regularly spaced ring-shaped film, or axially asymmetric wavy film. Serizawa et al. (2002) observed dispersed bubbly flow in a 25 μm microchannel at a superficial gas velocity of $j_G = 0.0083$ m/s, but such a low gas flow rate could not be readily measured in this work and bubbly flow was rarely detected for $j_G > 0.1$ m/s and $j_L < 4$ m/s (100 μm channel) or $j_L < 2$ m/s (50 μm channel).

The serpentine-like gas core described earlier for 530 and 250 μm channels was also observed in the 100 and 50 μm microchannels, although the level of interfacial deformation was incomparably smaller. At high liquid and gas flow rates, the multiple flow pattern was observed in the 100 μm

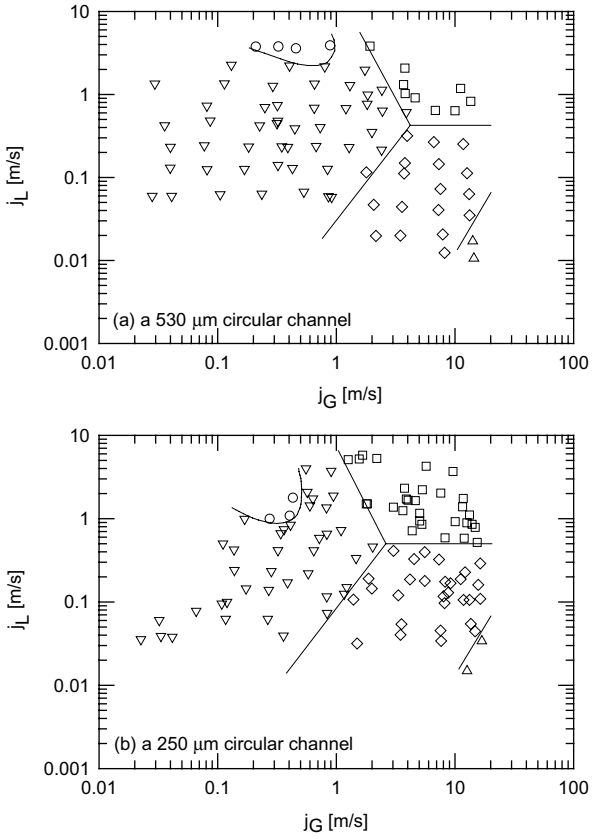

Fig. 6. Two-phase flow regime maps using flow pattern definitions for minichannels ((○) bubbly; (▽) slug; (□) churn; (◇) slug–annular; (△) annular; —transition lines).

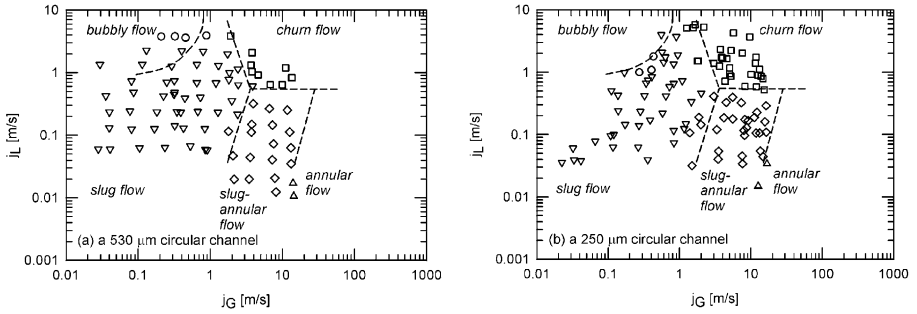

Fig. 7. Comparison of flow pattern data with Triplett et al.'s (1999) map for a minichannel ((○) bubbly; (▽) slug; (□) churn; (◇) slug–annular; (△) annular; --- transition lines by Triplett et al., 1999).

microchannel, featuring an alternating occurrence of liquid flow alone and gas slugs with different liquid film geometries, including a smooth, ring-shaped, and serpentine-like interface. The fre-

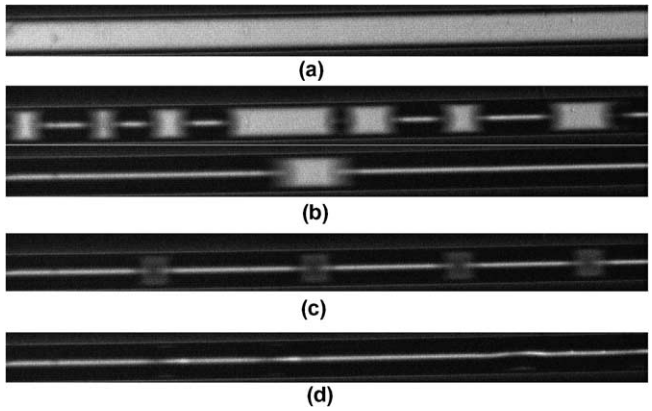

Fig. 8. Flow patterns in a 50 μm circular channel for the same flow conditions ($j_L = 0.38$ m/s and $j_G = 4.79$ m/s): (a) single-phase liquid flow; (b) gas slugs with thin-smooth liquid film; (c) gas slug with ring-shaped liquid film; (d) serpentine-like gas core.

quency of the serpentine-like gas core appearing was not sufficient for multiple flow to occur in the 50 μm microchannel.

It is evident that the dominant effects of surface tension and liquid viscosity in the 100 and 50 μm channels prohibit turbulence and agitation of the gas–liquid interface. As originally suggested by Kawahara et al. (2002), the absence of bubbly and churn flow in the 100 and 50 μm microchannels is probably due to the liquid flow remaining laminar. Despite the injection of gas into the liquid stream, there is insufficient turbulence generated in the liquid to break up the gas phase into small bubbles or create large amplitude waves at the gas–liquid interface. The meandering motion of the serpentine-like gas core is attributed to the lack of liquid turbulence, too.

Although liquid-ring flow was present in all of the channels, slug–annular flow was absent from the 100 and 50 μm channels. Recall that slug–annular flow is depicted by asymmetric waves of large amplitude that appear at the gas–liquid interface. The large asymmetric interfacial waves in the 530 and 250 μm channels become thin and axially symmetric in the 100 and 50 μm channels, due to the stronger influence of surface tension on the liquid film structure.

Annular flow was also absent from the 100 and 50 μm microchannels. It is speculated that the stronger surface tension effects in a microchannel allows the liquid film to bridge the gas core more easily than in a minichannel, so that the formation of annular flow would be less probable.

3.3. Flow pattern maps for horizontal microchannels

Recently, a new set of flow pattern definitions was introduced by Kawahara et al. (2002) to construct a flow regime map for the 100 μm circular channel. As shown in Fig. 8, the two-phase flow in a microchannel could be described as consisting of: (A) liquid alone; (B) gas core with a smooth liquid film; (C) gas core with a ring-shaped liquid film and (D) gas core with a deformed liquid film. This classification reduced the two-phase flow to a gas slug surrounded by a liquid film of distinct gas–liquid interface configurations (types B–D). From the recorded images for a given flow condition, the probability of each flow description occurring in the channel was computed.

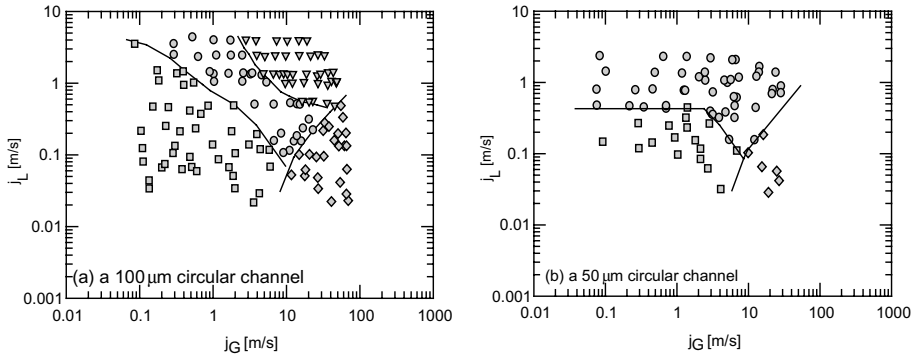

Fig. 9. Two-phase flow regime maps using flow pattern definitions of Kawahara et al. (2002) for microchannels ((■) slug–ring; (●) ring–slug; ▼ multiple; (◆) semi-annular; (—) transition lines).

Based on these probabilities and the time-averaged void fraction, ε, for a particular flow condition, four flow patterns were defined as follows: "slug–ring flow" occurs when the probability of class B is larger than that of C and ε is less than a preset value, e.g., 0.8; "ring–slug flow" occurs when the probability of class C is greater than that of B and $\varepsilon < 0.8$; "semi-annular flow occurs when the flow mostly alternates between classes A, B and C and $\varepsilon > 0.8$; and "multiple flow" occurs when the flow alternates between all four classes, A–D, and $\varepsilon < 0.8$.

The flow pattern maps for the 100 and 50 μm microchannels based on Kawahara et al.'s (2002) classification scheme are plotted in Fig. 9. The multiple flow pattern appeared at high gas and liquid flow rates in the 100 μm channel, but was replaced by the ring–slug flow pattern in the 50 μm channel. The other two flow patterns (slug–ring and semi-annular) were relatively unaffected by the channel diameter. The gravitational force and inertia are diminished with a reduction in the channel diameter, while the surface tension effect and viscous force are enhanced. At high gas and liquid flow rates, the liquid lump that normally collects under the serpentine-like gas core is distributed uniformly around the slug perimeter in the 50 μm channel, so the gas slug is unable to exhibit a serpentine-like distorted interface, a feature of multiple flow.

The transition line between slug–ring flow and ring–slug flow in the 100 μm channel is also different at low gas and high liquid flow rates from that drawn in the 50 μm channel. Although little is known about the formation of the ring-shaped liquid film, it is considered to be related to an interfacial instability dependent on a balance between surface tension and gas/liquid inertia.

3.4. Void fraction

Different methods of image analysis were used in determining the space and ensemble-average void fraction from the video images of the gas–liquid interface. The void fraction data in the 530 and 250 μm channels were deduced from about 300 video images in each experimental run. Initially, these images were sorted by flow pattern into nine categories: (a) liquid alone; (b) gas bubble; (c) short gas slug; (d) long gas slug; (e) liquid slug; (f) nose of gas slug; (g) tail of gas slug; (h) liquid ring and (i) deformed interface. The void fraction was calculated by fitting the region occupied by gas to shapes of symmetrical volume and estimating the fraction of gas volume.

To estimate the void fraction in the 100 and 50 μm microchannels, image analysis was performed on 200–500 video images in each run. The images were assigned a void fraction of zero when they depicted liquid flowing alone or a void fraction of unity when they depicted gas core flow with a thin-smooth liquid film or ring-shaped liquid film. This assignment works because the gas core flow in the images always fills the whole axial field-of-view. For a thick-smooth liquid film, the volume fraction of gas was estimated by squaring the ratio of the gas core radius to the channel radius (Kawahara et al., 2002). The effect of optical distortion on the abovementioned method of measuring the void fraction, particularly for gas core flows with ring-shaped films and thick liquid films, was already addressed by Kawahara et al. (2002).

Fig. 10 presents the time-averaged void fraction, ε, plotted against the volumetric quality, β, for all four microchannel sizes. The void fraction expression for homogeneous flow ($\varepsilon = \beta$) and the correlation for narrow channels ($\varepsilon = 0.8\beta$) recommended by Ali et al. (1993) for narrow channels of $D_H \sim 1$ mm are shown as a dotted and dashed line in the figures, respectively. Both show a linear relationship between the void fraction and volumetric quality. The void fraction for the 530 μm channel is predicted well by the homogeneous flow model, while that for the 250 μm channel agrees favorably with the Armand-type correlation recommended for a minichannel. On the contrary, the void fraction data for the 100 and 50 μm microchannels do not correlate with either the homogeneous flow model or an Armand-type correlation. The void fraction-to-volumetric quality relationship is instead non-linear. The void fraction increases slowly with increasing volumetric quality and then exponentially after $\beta = \sim 0.8$. This trend implies a strong departure

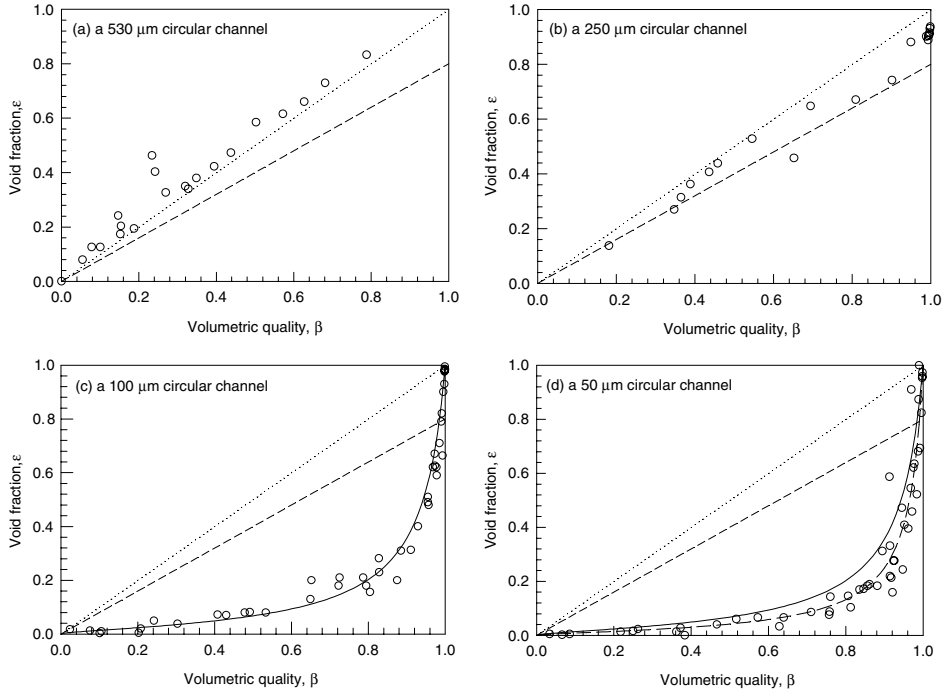

Fig. 10. Relationship between void fraction and volumetric quality ((○) measured; (—) Eq. (27) with $C_1 = 0.03$, $C_2 = 0.97$; (– – –) Eq. (27) with $C_1 = 0.02$, $C_2 = 0.98$; (· · ·) homogeneous flow; (- - -) Ali et al., 1993).

from homogeneous flow and indicates a large velocity slip between the liquid and gas phases. A physical interpretation of the large velocity slip is discussed shortly. Subsequently, the following empirical correlation was fitted to the void fraction data for the 100 and 50 μm channels and is plotted as a solid curve in Fig. 10:

$$\varepsilon = \frac{C_1 \beta^{0.5}}{1 - C_2 \beta^{0.5}}, \tag{1}$$

where C_1 and C_2 are constants based on the experimental results. $C_1 = 0.03$ and $C_2 = 0.97$ for the 100 μm circular channel; $C_1 = 0.02$ and $C_2 = 0.98$ for the 50 μm circular channel.

It is obvious that as the channel diameter is reduced from 100 to 50 μm, the void fraction is further reduced at a given volumetric quality. The physical reason why the relationship between ε and β in a microchannel deviates from the conventional linear relationship for a minichannel may be explained as follows. In a microchannel, between $\beta = 0$ and 0.8, the void fraction data fell below traditional correlations developed for minichannels and conventional channels. At these volumetric qualities, short gas slugs and long liquid slugs appeared. The long liquid slugs would increase the pressure gradient which would in turn cause the short gas slugs to accelerate through the liquid evading capture by the video camera and decreasing their residence time in the microchannel, which results in a low time-averaged void fraction.

Above a volumetric quality of 0.8, the void fraction rapidly approaches the values expected in larger channels. At large volumetric qualities, the gas flow rate is much higher than the liquid flow rate, resulting in gas slugs that are longer or occurring more frequently. As the gas slugs occupy more of the microchannel volume, the pressure gradient decreases and the gas slugs move less rapidly. As the residence time of the gas slugs increases, there is a greater probability of them being recorded by the camera (high void fraction). With shorter or fewer liquid slugs present, the pressure gradient along the channel is reduced as well.

On the other hand, in minichannels, the gas–liquid interface is more wavy and deformed, and the gas slugs experience far greater momentum exchange with the liquid accordingly. The enhanced momentum transfer actually hampers the gas slugs from speeding through the liquid, so the void fraction remains much higher than in microchannels.

3.5. Two-phase frictional pressure drop

Traditional models that assume a homogeneous or separated flow were applied to measurements of the two-phase frictional pressure drop in all of the test channels. In addition, a new theoretical model was developed to predict the two-phase frictional pressure gradient in the 100 and 50 μm microchannels. In the analysis of two-phase frictional pressure drop, the single-phase friction factor is required. Experiments using just de-ionized water were conducted first in all four channels to collect the single-phase pressure drop data. The single-phase friction factor obtained from the pressure drop data agreed well with the conventional correlation for laminar flow in a circular tube. Also, the laminar-to-turbulent transition for the 100–530 μm channels was found to occur at about the same critical Reynolds number as in larger channels.

3.5.1. Homogeneous flow model

Previously, the homogeneous flow model has predicted the two-phase frictional pressure drop in minichannels with success, e.g., for ammonia-steam flow in circular minichannels with $D = 1.46$–3.15 mm (Ungar and Cornwell, 1992) and for air–water flow in circular and semi-triangular minichannels with $D_H = 1.09$ and 1.49 mm (Triplett et al., 1999). Nonetheless, the recurring images of long gas slugs (relative to channel diameter) and large velocity slip ratios in microchannels imply that the two-phase flow can not be treated as a homogeneous flow in the 100 and 50 μm microchannels.

In the homogeneous flow model, the two-phase Darcy friction factor used to calculate the two-phase pressure gradient is a function of the homogeneous Reynolds number, which depends on the two-phase mixture viscosity, μ_H. Several different models have been proposed to evaluate the two-phase viscosity. Kawahara et al. (2002) were able to predict (within ±20%) the two-phase pressure gradient data for a 100 μm microchannel using Dukler et al.'s (1964) viscosity model:

$$\mu_H = \beta\mu_G + (1-\beta)\mu_L, \tag{2}$$

where μ_H is the homogeneous mixture viscosity. For narrow channels of $D_H \sim 1$ mm, Ali et al. (1993) found the viscosity model of Beattie and Whalley (1982) to be applicable for predicting the two-phase pressure drop:

$$\mu_H = \mu_L(1-\beta)(1+2.5\beta) + \mu_G\beta. \tag{3}$$

Figs. 11 and 12 compare the present two-phase pressure gradient data with the predictions of the homogeneous flow model with Eqs. (2) and (3), respectively. Dukler et al.'s (1964) viscosity

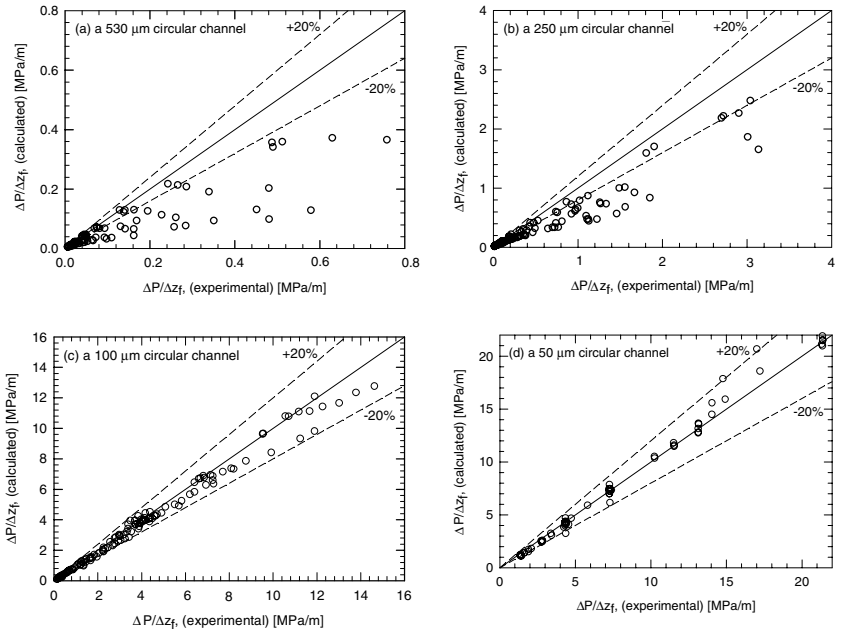

Fig. 11. Predictions of two-phase pressure gradient data by a homogeneous flow model with Dukler et al.'s (1964) viscosity correlation.

correlation predicts the data poorly for the 530 and 250 μm channels, yet produces reasonable agreement (within ±20%) with the 100 and 50 μm microchannel data. On the other hand, the homogeneous flow model with Beattie and Whalley's (1982) mixture viscosity correlation roughly predicts the two-phase pressure gradient data for the 530 and 250 μm channels but significantly over-predicts the data for the 100 and 50 μm channels (Fig. 12).

For a given homogeneous void fraction, β, Beattie and Whalley's (1982) model estimates a consistently higher mixture viscosity than that predicted by Dukler et al.'s (1964) model. Thus, it is intuitive that a better estimate of the two-phase pressure drop is obtained for the 530 and 250 μm channels with Beattie and Whalley's (1982) model. A higher mixture viscosity will compensate for the added pressure loss due to mixing of the two phases, as evident from the bubbly and churn flow patterns identified earlier in the 530 and 250 μm channels. In contrast, the laminar flows of gas and liquid in the 100 and 50 μm microchannels do not warrant any enhancement in the mixture viscosity to account for mixing, so better predictions of microchannel data are obtained with Dukler et al.'s (1964) viscosity model.

3.5.2. Separated flow model

Assuming separated flow, Lockhart and Martinelli (1949) defined a two-phase friction multiplier to relate the two-phase pressure gradient to the single-phase pressure gradient for liquid flow. They defined the Lockhart–Martinelli parameter, X^2, as the ratio of the single-phase liquid and

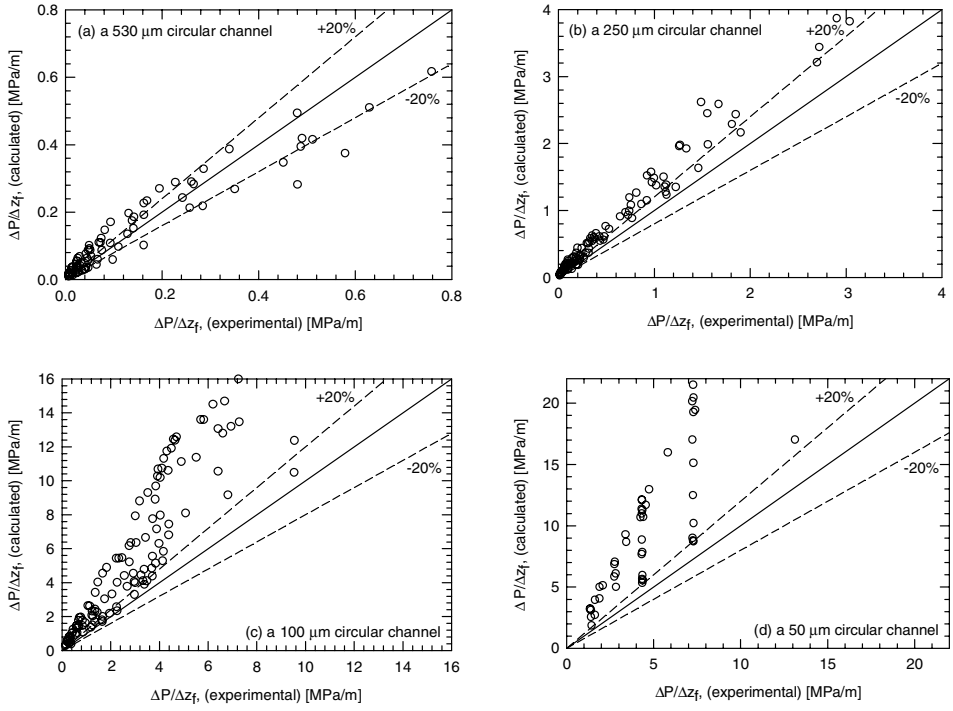

Fig. 12. Predictions of two-phase pressure gradient data by a homogeneous flow model with Beattie and Whalley's (1982) viscosity correlation.

gas pressure gradients, and graphically represented the relationship between the friction multiplier, ϕ^2, and Lockhart–Martinelli parameter. Chisholm and Laird (1958) related the friction multiplier to the Lockhart–Martinelli parameter through a simple expression that depends on the coefficient C ranging from 5 to 20, depending on laminar or turbulent flow of gas and liquid.

$$\phi_L^2 = 1 + \frac{C}{X} + \frac{1}{X^2} \tag{4}$$

Mishima and Hibiki (1996) and Lee and Lee (2001) also developed different correlations for the C-value based on the air–water two-phase flow data obtained in small channels, with D_H from 1 to 4 mm, and 0.78 to 6.67 mm, respectively.

The separated flow model has enjoyed success in predicting the two-phase pressure drop in small channels and for stratified flow in horizontal pipelines. The separated flow model was tested successfully for air–water flow in miniature triangular channels with $D_H = 0.87$–2.89 mm (Zhao and Bi, 2001b), and for nitrogen gas–water flow in both a circular channel with $D = 100$ μm (Kawahara et al., 2002) and a square channel with $D_H = 96$ μm (Chung et al., in press).

Fig. 13 shows the two-phase friction multiplier data plotted against the Lockhart–Martinelli parameter for the 50–530 μm channels. The spread of data points for the 250 and 530 μm channels

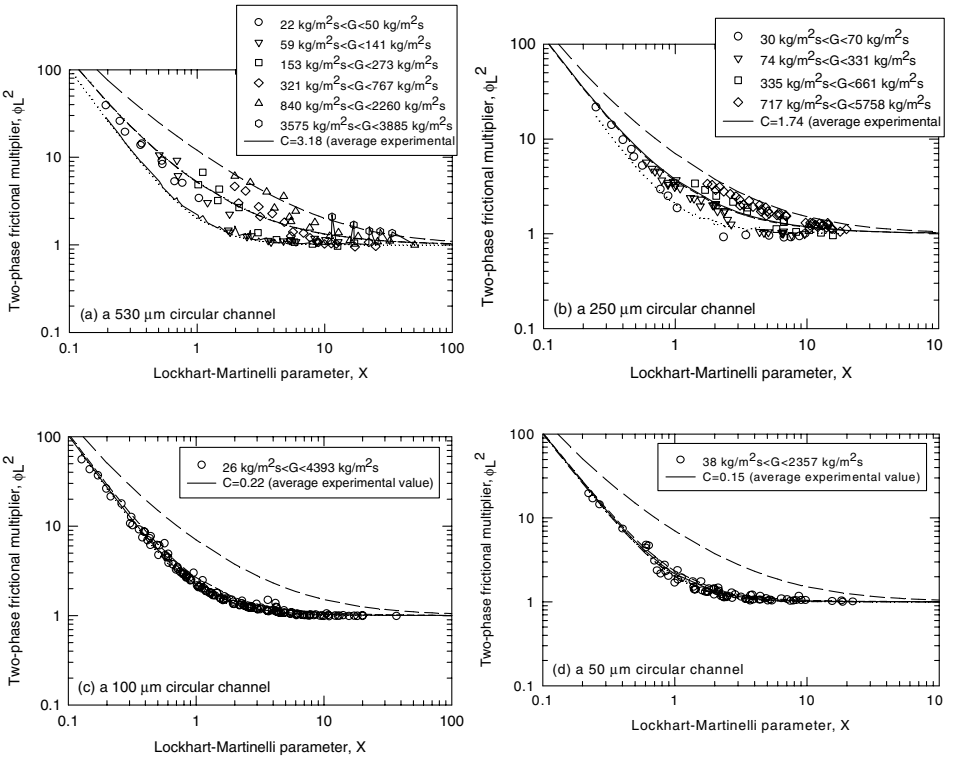

Fig. 13. Variation of the two-phase friction multiplier with the Lockhart–Martinelli parameter ((– – –) $C = 5$ from Chisholm (1967); (- · - · - · -) $C = 10$ from Chisholm (1967); (- - -) C from Mishima and Hibiki, 1996; (—) C from average experimental value; (· · ·) C from Lee and Lee, 2001; (- · - · - · -) $C = 0$).

(Fig. 13a and b) is suggestive of a mass flux effect on the friction multiplier, a feature common to minichannels of $D_H \geqslant 1$ mm (Kawaji, 1999). Each range of mass flux requires a different C-value and there is no single value of C that would satisfactorily predict this dependency of the friction multiplier on the mass flux. Conversely, the friction multiplier data collapse into a single curve for all mass fluxes measured in the 100 and 50 μm microchannels (Fig. 13c and d). Only one value of C, equal to 0.22 for 100 μm or 0.15 for 50 μm microchannels, is needed to correlate the friction multiplier data for the microchannels in terms of the Lockhart–Martinelli parameter.

For the 100 and 50-μm microchannels, the two-phase friction multiplier could also be predicted within ± 10% by the C-value correlations of Lee and Lee (2001), and Mishima and Hibiki (1996), while those obtained using $C = 5$, as proposed by Chisholm and Laird (1958) for conventional channels would overestimate the data by much more.

From the above results, the applicable value of C is seen to decrease as the channel diameter is reduced from 530 to 50 μm. It is noted that the C-value for microchannels of diameter less than 50 μm would be practically zero, which corresponds to the case of a completely separated laminar flow of gas and liquid with minimal momentum coupling between the two phases (Ali et al., 1993).

3.6. Model of two-phase flow in microchannels

Garimella et al. (2002) developed a mechanistic model to estimate the frictional pressure drop for intermittent flow during condensation of the refrigerant R134a in a horizontal circular channel. They showed 88% of the predictions to be within 25% of the experimental data for five minichannels of 0.506–4.01 mm in diameter. Their model is modified here to calculate the pressure drop gradient for the 50 and 100 μm microchannels tested here. Unlike Garimella et al. (2002), the modified model was applied to all flow conditions and ensuing flow patterns in the microchannels, since the flow patterns in a microchannel of 100 μm diameter have been observed to be entirely intermittent (Kawahara et al., 2002). In a later section, the theoretical predictions are validated by the measured results.

Some of the assumptions made in Garimella et al.'s (2002) model and the present model were asserted earlier by Suo and Griffith (1964) and Fukano et al. (1989). The present model assumes the flow to be completely intermittent and composed of unit cells (UC), each unit cell consisting of a gas slug immersed in liquid as shown in Fig. 14. The unit cell is then divided into two regions: one region occupied by the single-phase flow of liquid and the other by the two-phase flow of liquid and gas. In the single-phase region, the liquid has no entrained gas bubbles. In the two-phase region, a gas slug is cylindrical in shape and surrounded by an annular liquid film. The thin liquid film is assumed to be of uniform thickness around the channel circumference due to the diminishing role of gravity and growing importance of surface tension at smaller channel sizes. However, inertia continues to be the dominating force. The gas slug is assumed to be axially symmetric and travel through the slowly moving liquid slugs, which enclose the gas slug from the front and behind. Near the channel wall, the liquid film around the gas slug travels much slower than the liquid and gas slugs due to the viscous effect.

In the present model, the total pressure drop is given by the summation of the frictional pressure drop attributed to each region. Although Garimella et al. (2002) followed Dukler and Hubbard (1975) and assumed that pressure is additionally lost by the acceleration of the liquid film at the tail of the gas slug and subsequent mixing with the liquid slug behind, this contribution

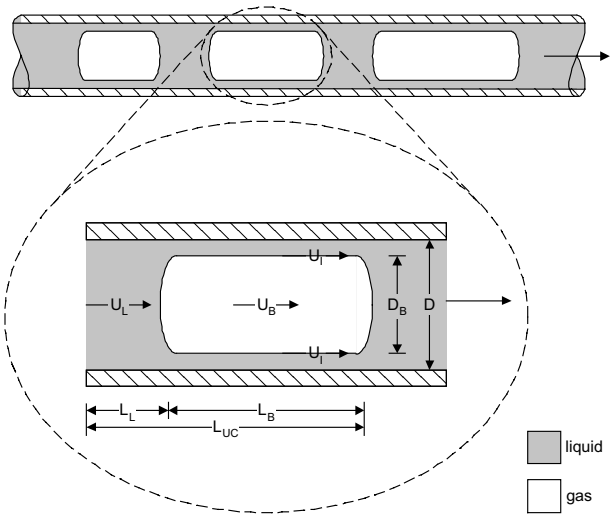

Fig. 14. Diagram of unit cell for model.

is assumed to be negligibly small in the 50 and 100 μm microchannels, as the liquid flow is typically slow and laminar, and mixing is suppressed. Therefore, the proposed model should not be used for channels with diameters greater than 100 μm. Not knowing the number of unit cells nor length, L_{UC}, or frequency of the unit cell, Garimella et al. (2002) relied on an empirical correlation for the number of unit cells to fit the calculated results to that measured. By doing so, the significance of such pressure drop remains unresolved.

3.6.1. Pressure drop in the single-phase region

The average velocity, U_L, and Reynolds number, Re_L, of the liquid slug can be evaluated from the experimental values of the superficial liquid velocity, j_L, and average void fraction, ε:

$$U_L = \frac{j_L}{1-\varepsilon}, \tag{5}$$

$$Re_L = \frac{\rho_L U_L D}{\mu_L}. \tag{6}$$

As the liquid slug moves like a single-phase flow, the pressure gradient in the liquid slug is given by the Darcy–Weisbach equation:

$$\left(\frac{dP}{dz}\right)_L = f_L \frac{\rho_L U_L^2}{2D}, \tag{7}$$

where $(dP/dz)_L$ and f_L are the corresponding pressure gradient and friction factor for the liquid slug. The friction factor for laminar flow ($Re_L < 2100$) in a circular channel is

$$f_L = \frac{64}{Re_L}. \tag{8}$$

The Blasius formula yields the friction factor for turbulent flow ($4000 < Re_L < 100,000$) in a smooth channel:

$$f_L = \frac{0.3164}{Re_L^{0.25}}. \tag{9}$$

For the liquid slug undergoing transition from laminar to turbulent flow ($2100 \leqslant Re_L \leqslant 4000$), the model uses the Blasius equation to obtain the friction factor.

3.6.2. Pressure drop in the two-phase region

Some researchers (Fukano et al., 1989; Suo and Griffith, 1964; Dukler and Hubbard, 1975) have neglected the importance of the pressure drop in the two-phase region to the total pressure drop. Nevertheless, the contribution of the two-phase pressure drop was included in the present model in acknowledgement of the greater pressure drop experienced in the microchannels than the minichannels and conventional channels of the authors cited above.

The model takes the average velocity of the gas slug, U_B, and gas phase, U_G, to be equivalent:

$$U_B = U_G, \tag{10}$$

where

$$U_G = \frac{j_G}{\varepsilon}. \tag{11}$$

On the contrary, Garimella et al. (2002) made the assumption that $U_B = 1.2U_S$ in their model, where U_S is the average velocity of the liquid slug, given by the sum of the superficial liquid and gas velocities (Suo and Griffith, 1964). The assumed relationship between the liquid and gas slug velocities is actually the same as the Armand expression (1946) for void fraction ($U_B = 1.2U_S \rightarrow j_G/\varepsilon = 1.2(j_L + j_G) \rightarrow \beta/\varepsilon = 1.2 \rightarrow \varepsilon = 0.833\beta$).

The Reynolds number of the gas slug, Re_B, is defined by

$$Re_B = \frac{\rho_G(U_B - U_I)D_B}{\mu_G}, \tag{12}$$

where the average velocity of the gas–liquid interface, U_I, is unknown. The model assumes that the flow of the gas slug is driven by the pressure gradient alone.

Once the velocity profile for the gas slug is known and the no-slip and wall shear stress boundary conditions specified, the average interface velocity can be expressed by:

$$U_I = \frac{\left(\frac{dP}{dz}\right)_{F/B}}{16\mu_L}(D^2 - D_B^2). \tag{13}$$

Here, the pressure gradient in the two-phase region, $(dP/dz)_{F/B}$, is approximated by

$$\left(\frac{dP}{dz}\right)_{F/B} = f_B \frac{\rho_G(U_B - U_I)^2}{2D_B} \tag{14}$$

and the friction factor for the gas slug, f_B, is determined in exactly the same way as was described for the liquid slug. The derivation of this equation is documented in greater depth by Garimella et al. (2002).

Garimella et al. (2002) calculated the bubble diameter to occupy about 90% ($0.899 \leqslant D_B/D \leqslant 0.911$) of the tube diameter, typical of minichannels. For computational simplicity, the model presented here assumes that

$$D_B = 0.90D \tag{15}$$

for all flow conditions. The unknown variables remaining are Re_B, U_I, and $(dP/dz)_{F/B}$. Eqs. (12)–(14) can then be solved for the three unknown variables. Ultimately, an iterative scheme was adopted to solve for the two-phase pressure gradient because of the implicit nature of the equations.

3.6.3. Relative lengths of the single and two-phase regions

In addition to the pressure gradients of the single and two-phase regions, the relative lengths of these regions in the unit cell must be known. Garimella et al. (2002) implemented the correlation of Fukano et al. (1989) for the relative length of the liquid slug in their pressure drop model. Since the correlation by Fukano et al. (1989) was developed for two-phase flow in minichannels with diameters of 1.0–4.9 mm, it may not be applicable to the microchannels of interest. Thus, the length of each region was inferred from the measured void fraction data in the present model. Neglecting the round nose and tail, the length of the gas slug, L_B, or two-phase region is related to the length of the unit cell, $L_{UC} = L_L + L_B$, by void fraction like so: $[(\pi D_B^2 L_B/4)/(\pi D^2 L_{UC}/4) = \varepsilon \rightarrow L_B = \varepsilon L_{UC}(D/D_B)^2]$. Hence, the relative lengths of the gas slug (L_B/L_{UC}) and liquid slug (L_L/L_{UC}) are given by

$$\frac{L_B}{L_{UC}} = \varepsilon\left(\frac{D}{D_B}\right)^2 \tag{16}$$

$$\frac{L_L}{L_{UC}} = 1 - \frac{L_B}{L_{UC}}. \tag{17}$$

Next, the product of the pressure gradient and relative length in each region is added together to give the total pressure gradient, $(dP_f/dz)_{TP}$, across the whole unit cell:

$$\left(\frac{dP_f}{dz}\right)_{TP} = \left(\frac{dP}{dz}\right)_{F/B}\frac{L_B}{L_{UC}} + \left(\frac{dP}{dz}\right)_{L}\frac{L_L}{L_{UC}} \tag{18}$$

Finally, the model is validated by comparing the predicted values of the total frictional pressure gradient to those measured.

3.7. Model predictions for microchannels

Based on the slug flow pattern, a mechanistic model for two-phase flow in microchannels was developed to gain insight into the strong deviation of the void fraction data from a linear relationship with volumetric quality, traditionally seen in minichannels. The model predicts the two-phase pressure drop using experimental conditions for the input parameters, including void fraction data. Since slug flow is assumed, the proposed model is only applied to the test results for the 100 and 50 μm microchannels, as shown in Fig. 15.

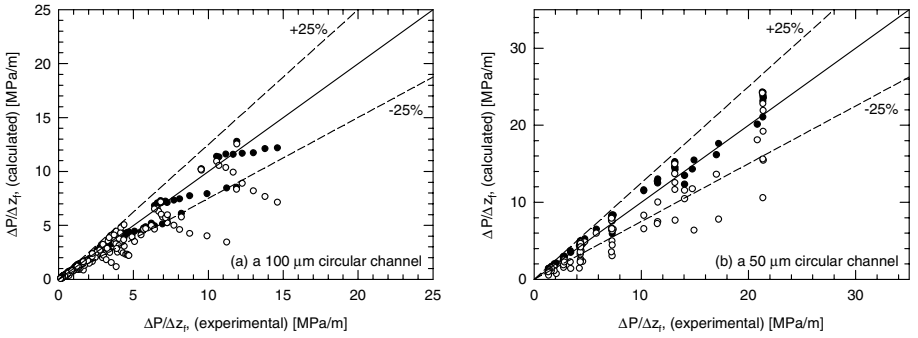

Fig. 15. Comparison of model predictions with experimental results for the two-phase pressure drop in microchannels ((●) using experimental void fraction; (○) using void fraction from the Armand (1946) correlation).

The model predictions display a closer fit to the measured data for a smaller channel diameter ($D = 50$ μm) due to the absence of the multiple flow pattern, which was present in the 100 μm channel. To demonstrate further the inadequacy of conventional void fraction relations for the 100 and 50 μm channels, predictions of the present model using the void fraction from the Armand (1946) correlation ($\varepsilon = 0.83\beta$) are also shown in Fig. 15, which reveals poor agreement with experimental data.

The successful predictions of the present slug flow model indicate that the two-phase flow in a microchannel of 100–50 μm diameter can be regarded as consisting of gas slugs speeding through liquid in a microchannel. The gas slugs of various lengths move rapidly through the liquid at such a rate that many parts of the microchannel are occupied by single-phase liquid moving slowly, yielding a large slip ratio between the gas and liquid. The unexpectedly low void fraction data obtained in 100 and 50 μm diameter channels were shown to support the present two-phase flow model for microchannels since the model predictions agreed well with the measured two-phase pressure drop data.

4. Conclusions

Two-phase flow experiments were carried out with nitrogen gas and water in circular channels of 530, 250, 100, and 50 μm diameter. The gas and liquid flow rates were varied and images of the two-phase flow patterns captured. Two-phase friction pressure drop data and void fraction data were also obtained. A slug flow model was developed and used to examine the two-phase pressure drop in microchannels. Pertaining to the fundamental issue of a scaling effect on two-phase flow, the following conclusions can be drawn.

For channels of $D_H = 250$ and 530 μm, the flow patterns observed were consistent with those appearing in minichannels of $D_H \sim 1$ mm: bubbly, slug, churn, slug–annular and annular flow. For channels of $D_H = 50$ and 100 μm, essentially only slug flow was identified under the flow conditions investigated. The absence of bubbly, churn, slug–annular and annular flow in channels of $D_H \leqslant 100$ μm was attributed to the greater viscous and surface tension effects on the liquid flow.

For channels of $D_H \geqslant 250$ μm, the time-averaged void fraction was comparable to that for minichannels of $D_H \sim 1$ mm, complying with the linear Armand (1946) correlation. For channels of $D_H \leqslant 100$ μm, the time-averaged void fraction was generally low, but increased exponentially at high volumetric quality (especially for $\beta > 0.8$), suggesting larger velocity slip ratios and weaker momentum coupling between the liquid and gas phases. This low void fraction measurement was consistent with the frequent images of liquid-only flow in the channels with $D_H \leqslant 100$ μm.

For channels of $D_H \geqslant 250$ μm, the two-phase frictional multiplier of Lockhart and Martinelli (1949) indicated a dependence on mass flux, analogous to that found in minichannels. Over each range of mass flux, a different C-value was required in the Chisholm and Laird (1958) correlation to fit the frictional multiplier. For channels of $D_H \leqslant 100$ μm, no dependence of the frictional multiplier on mass flux was detected and a common C-value could describe all the data well within ±20%.

The present results clearly revealed a channel diameter effect on two-phase flow. On the basis of the channel sizes tested, the two-phase flow characteristics changed significantly between 250 and 100 μm channel diameters. In channels with $D \leqslant 100$ μm, the two-phase flow characteristics are distinctly different from those in minichannels and conventional correlations no longer apply. However, since little is yet known about the effects of surface tension and liquid property on adiabatic two-phase flow in microchannels, the applicability of the present findings should be limited to similar gas–liquid pairs.

A new slug flow model is proposed for microchannels of $D_H \leqslant 100$ μm that can predict the two-phase frictional pressure gradient using the measured void fraction data. The successful application of this model further verified that the void fraction deviates from a conventional linear relationship with volumetric quality and supported the assumed notion of a gas slug quickly penetrating through the liquid which is held back by the effects of wall shear.

Acknowledgements

The authors wish to thank the Natural Sciences and Engineering Research Council of Canada for financially supporting the present work through Discovery Grant and Equipment grants. The authors are also grateful to the Government of Ontario for a graduate student scholarship for P.M.-Y. Chung.

References

Ali, M.I., Sadatomi, M., Kawaji, M., 1993. Two-phase flow in narrow channels between two flat plates. Can. J. Chem. Eng. 71, 657–666.

Armand, A.A., 1946. The resistance during the movement of a two-phase system in horizontal pipes, Izv. Vses. Teplotekh. Inst., 1, 16–23 (AERE-Lib/Trans 828).

Baker, O., 1954. Simultaneous flow of oil and gas. Oil Gas J. 26 (July), 185–195.

Beattie, D.R.H., Whalley, P.B., 1982. A simple two-phase flow frictional pressure drop calculation method. Int. J. Multiphase Flow 8, 83–87.

Chisholm, D., Laird, A.D.K., 1958. Two-phase flow in rough tubes. Trans. ASME 80, 276–286.

Chung, P.M.-Y., Kawaji, M., Kawahara, A., Shibata, Y., in press. Two-phase flow through square and circular microchannels—effect of channel geometry. ASME J. Fluids Eng.

Damianides, C.A., Westwater, J.W., 1988. Two-phase flow patterns in a compact heat exchanger and small tubes. In: Proceedings of Second UK National Conference on Heat Transfer, Glasgow, 14–16 September. Mechanical Engineering Publications, London, pp. 1257–1268.

Dukler, A.E., Hubbard, M.G., 1975. A model for gas–liquid slug flow in horizontal and near horizontal tubes. Ind. Eng. Chem. Fundam. 14, 337–347.

Dukler, A.E., Moye Wicks, Cleveland, R.G., 1964. Pressure drop and hold-up in two-phase flow. AIChE J. 10, 38–51.

Feng, Z.P., Serizawa, A., 1999. Visualization of two-phase flow patterns in an ultra-small tube. In: Proceedings of the 18th Multiphase Flow Symposium of Japan, 15–16 July, Osaka, Japan, pp. 33–36.

Fukano, T., Kariyasaki, A., 1993. Characteristics of gas–liquid two-phase flow in a capillary. Nucl. Eng. Des. 141, 59–68.

Fukano, T., Kariyasaki, A., Kagawa, M., 1989. Flow patterns and pressure drop in isothermal gas–liquid concurrent flow in a horizontal capillary tube. In: ANS Proceedings of the 1989 National Heat Transfer Conference, 6–9 August 1989, Philadelphia, Pennsylvania, HTC-Vol. 4, pp. 153–161.

Garimella, S., Killion, J.D., Coleman, J.W., 2002. An experimentally validated model for two-phase pressure drop in the intermittent flow regime for circular microchannels. J. Fluids Eng.—Trans. ASME 124, 205–214.

Joseph, D.D., Bai, R., Chen, K.P., Renardy, Y.Y., 1997. Core-annular flows. Annu. Rev. Fluid Mech. 29, 65–90.

Kandlikar, S.G., Grande, W.J., 2003. Evolution of microchannel flow passages—thermohydraulic performance and fabrication technology. Heat Transfer Eng. 24, 3–17.

Kawahara, A., Chung, P.M.-Y., Kawaji, M., 2002. Investigation of two-phase flow pattern, void fraction and pressure drop in a microchannel. Int. J. Multiphase Flow 28, 1411–1435.

Kawaji, M., 1999. Fluid mechanics aspects of two-phase flow: Flow in other geometries. In: Kandlikar, S.G., Shoji, M., Dhir, V.K. (Eds.), Handbook of Phase Change: Boiling and Condensation. Taylor & Francis, Washington DC, pp. 205–259.

Kawaji, M., Chung, P.M.-Y., in press. Unique characteristics of adiabatic gas–liquid flows in microchannels: diameter and shape effects on flow patterns, void fraction and pressure drop. Proceedings of the First International Conference on Microchannels and Minichannels, Rochester, New York, 24–25 April 2003. Int. J. Microscale Thermophys. Eng.

Kline, S.J., McClintock, F.A., 1953. Describing uncertainties in single sample experiments. Mech. Eng. 75, 3–8.

Lee, H.J., Lee, S.Y., 2001. Pressure drop correlations for two-phase flow within horizontal rectangular channels with small height. Int. J. Multiphase Flow 27, 783–796.

Lockhart, R.W., Martinelli, R.C., 1949. Proposed correlation of data for isothermal two-phase, two-component flow in pipes. Chem. Eng. Prog. 45, 39–48.

Madou, M.J., 2002. Fundamentals of microfabrication: the science of miniaturization. CRC Press, Boca Raton, FL.

Mishima, K., Hibiki, T., 1996. Some characteristics of air–water two-phase flow in small diameter vertical tubes. Int. J. Multiphase Flow 22, 703–712.

Serizawa, A., Feng, Z.P., 2001. Two-phase flow in micro-channels. In: Proceedings of the 4th International Conference on Multiphase Flow, May 27–June 1, 2001, New Orleans, LA, USA.

Serizawa, A., Feng, Z., Kawara, Z., 2002. Two-phase flow in microchannels. Exp. Therm. Fluid Sci. 26, 703–714.

Stanley, R.S., Barron, R.F., Ameel, T.A., 1997. Two-phase flow in microchannels. In: Micro-Electro-Mechanical Systems (MEMS), ASME, DSC-Vol. 62/HTD-Vol. 354, pp. 143–152.

Suo, M., Griffith, P., 1964. Two-phase flow in capillary tubes. J. Basic Eng. 86, 576–582.

Triplett, K.A., Ghiaasiaan, S.M., Abdel-Khalik, S.I., Sadowski, D.L., 1999. Gas–liquid two-phase flow in microchannels—Part I: Two-phase flow pattern. Int. J Multiphase Flow 25, 377–394.

Ungar, E.K., Cornwell, J.D., 1992. Two-phase pressure drop of ammonia in small diameter horizontal tubes. In: AIAA 17th Aerospace Ground Testing Conference, Nashville, TN, 6–8 July.

Zhao, T.S., Bi, Q.C., 2001a. Co-current air–water two-phase flow patterns in vertical triangular microchannels. Int. J. Multiphase Flow 27, 765–782.

Zhao, T.S., Bi, Q.C., 2001b. Pressure drop characteristics of gas–liquid two-phase flow in vertical miniature triangular channels. Int. J. Heat Mass Trans. 44, 2523–2534.